

Simulating Genetic Circuits in Bacterial Populations with Growth Heterogeneity

Anjan Roy^{1,2} and Stefan Klumpp^{1,2,*}

¹Max Planck Institute of Colloids and Interfaces, Potsdam, Germany and ²Institute for Nonlinear Dynamics, University of Göttingen, Göttingen, Germany

ABSTRACT We computationally study genetic circuits in bacterial populations with heterogeneities in the growth rate. To that end, we present a stochastic simulation method for gene circuits in populations of cells and propose an efficient implementation that we call the “Next Family Method”. Within this approach, we implement different population setups, specifically Chemostat-type growth and growth in an ideal Mother Machine and show that the population structure and its statistics are different for the different setups whenever there is growth heterogeneity. Such dependence on the population setup is demonstrated, in the case of bistable systems with different growth rates in the stable states, to have distinctive signatures on quantities including the distributions of protein concentration and growth rates, and hysteresis curves. Applying this method to a bistable antibiotic resistance circuit, we find that as a result of the different statistics in different population setups, the estimated minimal inhibitory concentration of the antibiotic becomes dependent on the population setup in which it is measured.

INTRODUCTION

Cellular functions and their adaptation to environmental conditions are to a large extent encoded in the regulatory connections of genetic circuits. Therefore, a quantitative understanding of the dynamics and the function of genetic circuits, combining predictive mathematical models with quantitative experiments and with the design of engineered circuits, is one of the key goals of systems biology (1–6). Specifically, a large body of work has addressed multistability (7–10) and stochastic effects (11–15), both of which result in heterogeneous gene expression in a genetically homogeneous population of cells.

One complication in the quantitative study of genetic circuits is that genetic circuits are usually coupled to the physiological state of the cell (16). The latter, for example, affects the availability of gene expression machinery and thereby influences the level of gene expression. In many cases, however, the expression status of a gene also has an effect on the cellular physiology; for example, in the case of essential enzymes limiting cell growth. This coupling has mostly been studied in bacteria in exponential growth phase, where the physiological state of the cell can often be characterized by the growth rate

(17,18). In the last 10 years such coupling has been demonstrated for a variety of genetic circuits (19–25). In these cases, heterogeneity in gene expression is accompanied by heterogeneity in cell growth with part of the population growing faster than the rest. For some genetic circuits, growth heterogeneity is a crucial part of their biological function; for example, bet hedging for survival in varying environments as proposed for the formation of bacterial persister cells (8,26), or for the heterogeneous expression of genes conveying resistance to antibiotics (23,27). In other cases, specifically in synthetic genetic circuits, growth heterogeneity may arise as an unavoidable and possibly unintended side effect of the desired function, but also allows for the implementation of more complex functions (22,28,29).

To study the growth and the heterogeneity of populations of cells, various setups have been used. Traditionally, bacterial growth has been studied in batch cultures, where bacteria grow exponentially until the medium gets depleted (20,30), and in continuous cultures or the Chemostat, where exponential growth is maintained by continuously diluting the population by washing out cells with fresh medium (17,31,32) (Fig. 1 *a*). More recently, microfluidic devices have been developed to observe cell growth at the single cell level (33–36). These devices include a microfluidic version of a Chemostat (34) and the so-called Mother Machine, in which a cell is trapped in a dead-end channel

Submitted August 7, 2017, and accepted for publication November 17, 2017.

*Correspondence: stefan.klumpp@phys.uni-goettingen.de

Editor: Nathalie Balaban.

<https://doi.org/10.1016/j.bpj.2017.11.3745>

© 2017 Biophysical Society.

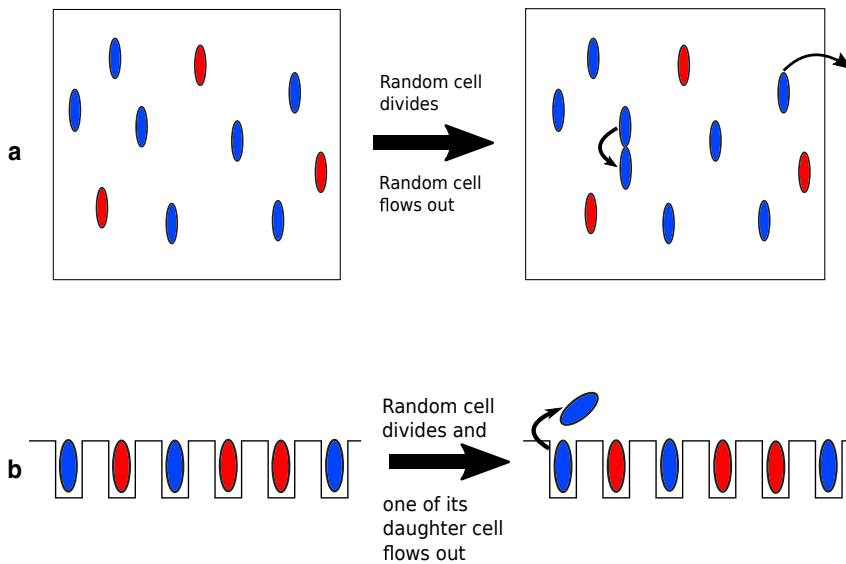


FIGURE 1 Schematic representation of the two population setups. The blue and red ellipsoids represent the two types of cells, fast and slow growing. (a) Chemostat-type growth. Dilution of the population is implemented by replacing a randomly chosen cell in the population with the newly formed daughter cell, whenever a cell divides. (b) Ideal Mother-Machine. Upon division, one of its daughter cells is flushed away whereas the other is kept. To see this figure in color, go online.

whereas its daughter cells are flushed away upon cell division, enabling the long-time study of individual cells (35) (Fig. 1 b).

By contrast, simulations of gene circuits have typically been carried out for single cells and analyzed with statistics over time using long trajectories rather than statistics over a population (37,38). These two types of statistical ensembles are usually equivalent, given sufficiently long trajectories and in the absence of growth heterogeneity. Growth heterogeneity, however, can be expected to result in the accumulation of the faster proliferating cells within a population, an effect not seen in the time statistics of a typical simulation. Indeed, the accumulation effect will in general depend on the type of experimental setup used, so that the statistical results for populations heterogeneous in growth may be different in different experimental setups. Recently, such an effect has been shown experimentally and discussed analytically for growth heterogeneity in a monostable system (39).

Here we present a method for stochastic simulations of genetic circuits in populations of growing cells, specifically populations that are heterogeneous in growth. The method is based on Gillespie's stochastic simulation algorithm (40,41), for which we propose a computationally efficient implementation, the Next Family Method; this is particularly suitable for a scenario with many cells. Within this approach, we implement Chemostat-type and Mother Machine-type population setups. We use a bistable mutual repression system with growth inhibited in one of the two states to demonstrate explicitly how growth heterogeneity results in different statistics in these two setups for commonly measured quantities such as subpopulation fractions, growth rates, and hysteresis curves. We then apply the method to study growth bistability in an antibiotic resistance system (23). In that case, we find a dependence of the

minimal inhibitory concentration (MIC) of the antibiotic, a parameter commonly used to quantify the effect of an antibiotic on bacterial populations, on the experimental setup.

METHODS

Simulating gene circuits in populations of growing cells

To simulate the dynamics of a genetic circuit in a population of growing cells, allowing also for the possibility of phenotype switching, we adapt Gillespie's stochastic simulation algorithm for a set of chemical reactions or other stochastic processes (40,41). In the Gillespie algorithm, each reaction (protein synthesis/degradation/dilution) is characterized by a propensity a_j corresponding to its reaction rate in the deterministic rate equation. These propensities determine the probabilities of the time, τ , when the next reaction will take place, and the type of reaction, j , which will take place at that time. There are multiple ways to generate τ and j . In the Direct Method, two random numbers are drawn in each step to determine the time and index of the next reaction, the simulation time is advanced to τ , the reaction j is carried out, and the reaction rates are updated for the next reaction to reflect changes in the copy number of relevant reactants.

This method can be applied directly to a population of cells, by considering reactions that occur in different cells as parallel reaction channels. Thus, for simulating a set of s reactions in a population of N cells, one has to evaluate sN propensities in total, and use them to calculate τ and j as before. This will give the time and the index of the next reaction happening in any of the N cells. However, to apply this method to a population of proliferating cells, we also need to account for cell division and to that end implement the different population setups. Implementing a growing population also means that the computational effort grows with increasing cell number. The implementation of the different population setups that we propose here also limits the increase of the cell number. Several different methods for limiting that increase are possible, and those correspond to different population setups and as we will show below, result in different predictions for experiments. Here, we specifically consider two setups of populations of proliferating cells that correspond to the ideal Mother Machine and the Chemostat. In both cases, we simulate a fixed population size N . In the first case, corresponding to an ideal Mother Machine,

every time a cell divides, we keep only one of its daughter cells. This is very similar to how simulations are done for a single cell (which corresponds to the special case $N = 1$). To implement this scenario, we do not need to describe the formation of the daughter cells through cell division explicitly, but only a dilution term for the proteins. In the second case, the Chemostat, we keep the population size constant by removing a random cell whenever a cell divides, mimicking the continuous dilution. This scenario corresponds to a variant of the Moran process (42), a stochastic model in evolution, with continuous time and a population with heterogeneous growth rates. In this case, an explicit description of the formation of daughter cells is required, because typically both cells remain in the population. We implement this production of daughter cells by introducing an additional propensity function $a_{s+1} = \lambda$ for each of the cells, with λ being the growth rate of that cell. This gives the probability that a cell divides into two daughter cells, both of which are in the same expression state and follow the original model for the dynamics of protein numbers. Whenever this reaction is selected, we produce an identical copy of the cell and replace a randomly selected member of the population with this copy, thereby mimicking the flushing out of cells and keeping the total number of cells (N) constant. We note that our method is not restricted to this Poissonian description of cell division. More detailed descriptions of cell division (with more realistic distributions of the division times) have been implemented in stochastic simulation of single cells (38), and can be implemented in our method for populations. One such case will be considered below.

Efficient implementation: the Next Family Method

The Gillespie algorithm using the Direct Method becomes quite slow when the number of reaction channels is large, as it spends a lot of computational time in determining the reaction channel j . Therefore, alternative but mathematically equivalent implementations have been developed. For example, in the First Reaction Method (41,43), the expected times are calculated for all individual reactions rather than just one, and the reaction to occur, i.e., the reaction number j , is determined by searching for the minimum among them. The reaction j is carried out and then the new time for that reaction is calculated. The Next Reaction Method (44) improves upon it by using an indexed heap data structure in which the reaction times are stored. This data structure generally speeds up sorting and finding a minimum (45), which is used here to determine the next reaction that occurs. However, the method loses this advantage when many of the reactions are coupled, so that the heap structure needs to be repaired for each of the coupled reactions when their corresponding reaction times are modified. A generalization, the First Family Method (43), partitions the reactions into families and then considers these families as pseudo-reactions. The First Reaction Method is then applied to determine which of these families or pseudo-reactions occur next and the Direct Method to determine the actual reaction within that family.

Even though the First Family Method was originally introduced mainly as a book-keeping method, in our case a natural classification of reactions into families is provided by the different cells. Moreover, as there is no interaction between the cells, these pseudo-reactions given by the grouped reactions in each cell are decoupled. We, therefore, calculate the expected time of next reaction for each of the N families (cells), heapify these reaction times so that any node has reaction times larger than its parent node (45), and identify the cell at the top of the heap as the one in which reaction will take place next. Once this reacting cell is identified, we can then use the Direct Method to find the actual reaction that occurs in that cell. A heap repair step is only required for this one cell in which reaction takes place. We note that if the reaction chosen is cell division and results in the production of a daughter cell in the case of Chemostat growth, one needs to perform an additional heap repair step on this new cell, which randomly replaces one of the existing cells (see the Supporting Material for more details). However, as long as there is no cross talk between different cells, this method, which may be called the Next Family Method, will be more efficient than any of the previous methods. Even under cross talk, it may

be possible to group the cells into modules that interact more among themselves than with cells of other modules, thereby making this current method quite powerful. In principle, this method can be generalized to any system where there are clustered reactions.

In Fig. 2, we demonstrate the significant speedup of simulations using the Next Family Method as compared to the Direct Method and the Next Reaction Method. Although the runtime scales as N^2 for the Direct Method, it scales as $N \log(N)$ for the Next Reaction Method as well as for the Next Family Method. Here, the first factor comes from the number of reactions occurring in a given time, which scales as N irrespective of the method used. The second factor comes from the time it takes to find j for each of the reaction steps. This scales as N for the Direct Method, which is the timescale required to scan through the propensities, and as $\log(N)$ for the Next Reaction and the Next Family Methods, which is the timescale required to repair the heap (45). As expected, there is a difference of a multiplicative factor between the runtimes of the Next Reaction and Next Family Methods. This difference corresponds to the extra heap repair steps needed for each of the coupled reactions and it will linearly increase with increasing number of coupled reactions. In Fig. S1, we show that the results obtained from these methods are statistically identical. We mention that other methods for implementing Gillespie's algorithm can also speed up the simulations. However, they either assume that some of the reactions can be introduced later (46) or that the reactions have widely different rates (47,48), neither of which is applicable in the situation we consider here.

RESULTS AND DISCUSSION

Test system: a toxic genetic toggle switch

To study the effect of the different growth setups on the observed behavior of growth heterogeneous systems, we first consider a bistable system with different growth rates in the two states. Specifically, we study a mutual repressor system or toggle switch with one toxic protein (Fig. 3 a). In a simple mutual repressor system, two proteins P_1 and P_2 repress the transcription of each other. This system is known to exhibit bistability: For sufficiently strong repression, there are two stable states. In one of them, the

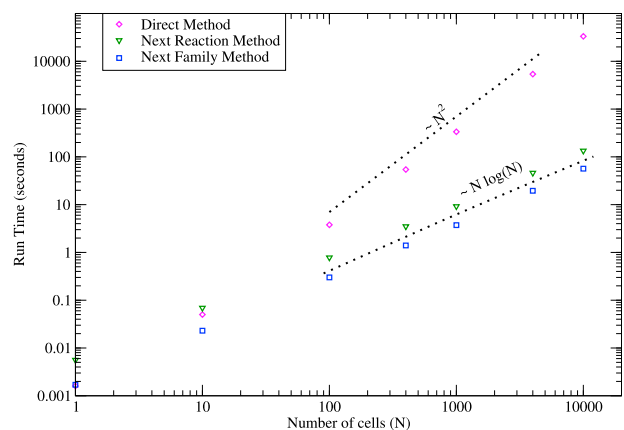


FIGURE 2 Speedup of simulations by the Next Family Method. Shown here are runtimes for a simulation of the toggle switch (see next section) in a Chemostat population of N cells, using the proposed Next Family Method (blue squares) as compared to that using the Direct Method (magenta diamonds) and the Next Reaction Method (green triangles), with all parameters being the same (in all these cases the system is evolved for 6000 min in total). To see this figure in color, go online.

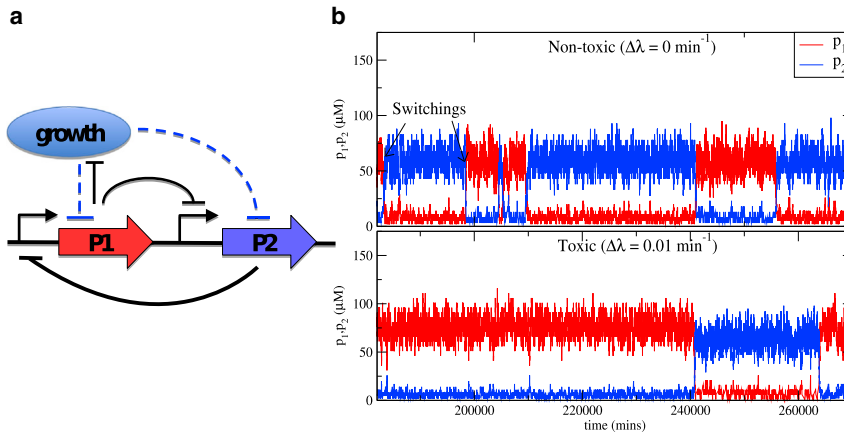


FIGURE 3 Toxic toggle switch. (a) Shown here is a schematic representation of the mutual repression circuit with growth inhibition by one of the two proteins (P_1). The black arrows represent specific gene regulation (here transcriptional repression), whereas the blue dashed arrows represent effects of the global state of the cell (*pointed arrowheads* are for positive regulation and *flat arrowheads* for negative). (b) Dynamics of the protein concentrations from simulations of a single cell without growth inhibition (*top*, $\Delta\lambda = 0 \text{ min}^{-1}$) and with growth inhibition by protein P_1 (*bottom*, $\Delta\lambda = 0.01 \text{ min}^{-1}$). Here we show a small segment of the whole temporal dynamics to clearly see the switching events. For the used parameters, see the [Supporting Material](#). To see this figure in color, go online.

concentration of P_1 (denoted by p_1) is high and the concentration of P_2 (denoted by p_2) is low; in the other, the roles are reversed (1). In simulations, a single cell switches stochastically between these two states (Fig. 3 b, upper panel). We modify this simple toggle switch by assuming that one of the proteins (say P_1) inhibits the growth of the cell, such that the growth rate of the cell is different in the two stable states. To keep the analysis simple, we describe the dependence of the growth rate on the concentration of P_1 by a simple interpolation between a maximal growth rate λ_{max} for small p_1 and a minimal growth rate λ_{min} for large p_1 . The strength of the growth inhibition is modulated by varying $\Delta\lambda = \lambda_{\text{max}} - \lambda_{\text{min}}$. Furthermore, we make the following simplifications: we consider the symmetric case, where both genes/proteins are characterized by the same parameters except for the growth inhibition, and growth is taken to affect gene expression only through dilution, neglecting a growth rate dependence of the protein synthesis rate (19) (see the [Supporting Material](#) for details). A scenario with more realistic assumptions is studied below. As a consequence of the symmetry of the parameters, a cell spends equal amounts of time in the high p_1 and high p_2 states in the absence of growth inhibition (Fig. 3 b, top panel). With increasing toxicity of P_1 , the reduction in growth rate in the high p_1 state leads to reduced dilution (reduced effective degradation rate of the proteins) and thereby increases the concentration of P_1 in the high p_1 state. As a consequence, the symmetry between the high p_1 and high p_2 states is broken. This in turn affects the rates of stochastic switching between the two states: a larger fluctuation is needed to switch from high p_1 to low p_1 than from high p_2 (low p_1) to low p_2 , making the cell spend more and more time in the slower growing (high p_1) state (Fig. 3 b, bottom panel).

We then simulated the dynamics of this genetic circuit for the two population setups with 1000 cells each, varying the growth rate difference $\Delta\lambda$ between the high p_2 and high p_1 states. The distribution of the concentration of protein P_1 obtained from the simulations for the three scenarios are

shown in Fig. 4. Due to the bistability of the genetic circuit, the distributions typically exhibit two (broad, but well-separated) peaks corresponding to the subpopulations with high and low p_1 (and low and high p_2). In the absence of a growth difference ($\Delta\lambda = 0$), the distributions are exactly the same for all three simulation scenarios. In addition, due to the symmetry of the parameters, the system spends an equal amount of time in the two states. This is reflected in the population fractions of the two states (obtained as the areas under the two peaks) being equal.

The distributions for a single cell show that with increasing growth difference, the population with high p_1 is shifted to even higher p_1 , and at the same time the probability of that subpopulation is increased. This reflects the observations made in Fig. 3 b above about the breaking of symmetry between the two states due to growth rate modulation.

The distribution obtained for the two population setups, which both coincided with the distribution for a single cell in the case $\Delta\lambda = 0$, are in general different from each other for $\Delta\lambda > 0$. As expected, the results for the population in an ideal Mother Machine is identical to those for a single cell for all values of $\Delta\lambda$. This is because the ideal Mother Machine is essentially an array of many individual cells and studying it is equivalent to taking an ensemble average over the individual cells (possibly in addition to a time average). The choice of one over the other is mostly a question of practicalities, e.g., if dynamics is observed over times in which no steady state is reached because of rare switchings, one might prefer statistics over a population. Note that even if sampling is done over all cells in a real Mother Machine with 10–20 cells per channel (most of which are flushed out after some time) rather than the one cell in our ideal Mother Machine (which is not flushed out), the results are very similar (Fig. S2). Therefore, in the rest of this study we will be referring to our ideal Mother Machine simply as the Mother Machine.

For the Chemostat, the results are quantitatively and qualitatively different. In the presence of a growth rate

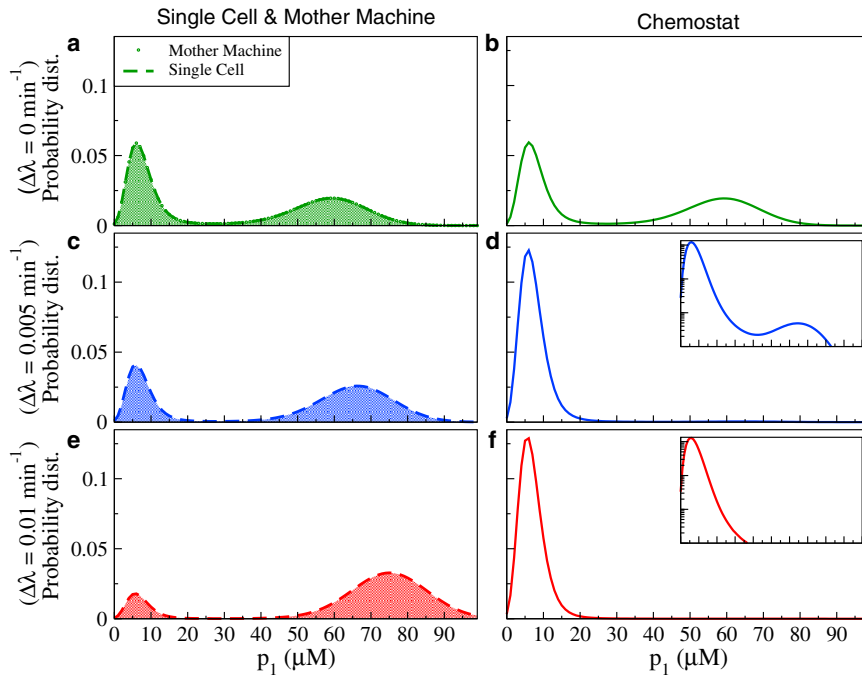


FIGURE 4 Distribution of the concentration of protein P_1 of the toxic toggle switch. Results are shown for three levels of growth inhibition by P_1 and three population scenarios. (a, c, and e) Single cell (dashed curves) and Mother Machine (shaded down curves). (b, d, and f) Chemostat (solid curves). The insets in (d) and (f) plot the same data on a log-linear scale to show the existence or absence of the small second peak. Sampling is done over 10^8 time steps of 5 min each for the Single cell, and over $N = 1000$ cells and 10^7 time steps of 5 min for the two populations. The parameters are given in the Supporting Material. It can be seen that the distribution is identical for the Single cell and the Mother Machine (see text). To see this figure in color, go online.

difference, the dominant population is not the slow growing high p_1 subpopulation as in the single cell and the Mother Machine scenarios, but the fast growing low p_1 subpopulation. This can also be seen in Fig. S3 where we plot the distribution of the growth rates explicitly. This could be either because of the low p_1 state suddenly becoming more stable, which should not be the case as individual cells are still the same, or because there are more of these fast growing low p_1 cells. Indeed, unlike the Mother Machine where the daughter cells are washed away, a Chemostat has both daughter and mother cells in the population. As a result, a Chemostat population will contain more offspring of the fast growing cells than of the slow growing ones.

The distribution of switching times between the two states, defined as the time interval between two instances of p_1 and p_2 crossing each other in one cell, is plotted in Fig. S4. The switching times are seen to be exponentially distributed and symmetric between the two states for the nontoxic case. In the toxic case, as expected, the switching times from the slow to fast growing state gets increased. Again, we see that the results are identical for the single cell and the Mother Machine, apart from the noise.

In Fig. S5, we plot the hysteresis curves when the synthesis rate α_1 is modulated. Here, the switching to and from the low p_1 state happens at larger values of α_1 in the Chemostat than in the Mother Machine/Single cell, because in the low p_1 state the fast growing cells accumulate more by replacing the slow growing ones.

The subpopulation fractions for a bistable system with growth differences can be estimated with a two-state model originally used in the context of persister cells (8,49). This

model describes the population as consisting of two subpopulations (which in our case correspond to the high p_1 and high p_2 states) with different growth rates (λ_1 and λ_2) and with stochastic switching between the two subpopulations, but in contrast to our full model assumes the growth rate to have a unique sharp value in each state. In that case, the population fraction of the slow growing state (λ_2) is given by (49)

$$\frac{N_2}{N_1 + N_2} \approx \frac{k}{\lambda_1 - \lambda_2}, \quad (1)$$

where k is the switching rate from the fast growing to the slow growing state. The rate for switching in the opposite direction does not affect the population fractions. A simple interpretation of this relation is that the population fractions are determined by a balance between two processes: slow growing cells are outgrown by the fast growing cells, but the slow growing population does not disappear because it is continuously restored by switching of fast growing cells to the slow growing state. Simulating this two-state model with our method, we find excellent agreement between the population fractions obtained from the simulation and the prediction of this relation, as shown in Table 1. (We note that this agreement also provides a quantitative test of our simulation method.) In our full model, the distribution of the growth rate is not sharp, but we can extract the average single cell growth rates (λ_1 and λ_2) as well as the size of the two subpopulations (N_1 and N_2) from the Chemostat simulations shown in Fig. S3. The switching rates are estimated as the inverse of the average switching times in the Single

TABLE 1 Subpopulation Fraction of the Slow Growing State

Case	k	λ_1	λ_2	$N_2/(N_1 + N_2)$	$k/(\lambda_1 - \lambda_2)$
Two-state model	0.001	0.04	0.03	0.0983	0.1
Toggle switch with $\Delta\lambda = 0.01$	4.36×10^{-5}	0.03746	0.03268	4.2×10^{-3}	9.12×10^{-3}
Toggle switch with $\Delta\lambda = 0.005$	7.58×10^{-5}	0.03863	0.03623	1.7×10^{-2}	3.16×10^{-2}

Subpopulation fraction obtained directly from Chemostat simulation ($N_2/(N_1 + N_2)$) of the two-state system matches almost exactly with that estimated from the ratio of switching rate to the slow growing state (k) and relative growth rate of fast growing state ($\lambda_1 - \lambda_2$). For the toggle switch, the agreement is within a factor of 2.

cell or Mother Machine simulations (Fig. S4). Doing so, we still find agreement with Eq. 1 within a factor 2 (Table 1), which appears to result from the broad distribution of growth rates within the subpopulations.

So far, we have presented results for a highly simplified model with a very particular type of growth rate modulation. However, these qualitative results are generally expected whenever there is heterogeneity in the growth rate. As a test that the results are not dependent on the specific assumptions we have made, we also considered a more realistic model, in which the growth rate depends on the concentration p_1 through a Hill function. In that case, the toxicity of the protein P_1 is modulated by changing the threshold concentration (K_λ) of that Hill function. We also included a growth rate dependence of the protein synthesis rates (50) (see the Supporting Material for details). The results for this model are qualitatively the same as for the simplified model, as shown in Fig. S6. In particular, we observe again that growth heterogeneity (finite threshold K_λ) results in an increase of the slow growing (high p_1)

subpopulation in the Mother Machine, but to an increase in the fast growing (low p_1) subpopulation in the Chemostat.

Another aspect of our current model that is highly simplified is the description of cell division as a Poissonian process. More detailed descriptions can be implemented within our method. As an example, we have used a Gaussian distribution of division times, without correlations between subsequent generations. Fig. S7 compares the results in the Chemostat scenario for the two descriptions of division and shows that the differences between them are very small in this case. In general, however, the mechanism of division can affect the results. For example, in a recent study, Hashimoto et al. (39) concluded that for a system with a monomodal distribution of growth rates, the measured population doubling time is smaller than the mean doubling time of the constituent single cells, indicating a dominance of the faster growing cells. This conclusion was reversed in another recent study by Lin and Amir (51) by including correlations between the division times of mother and daughter cells that result from the underlying size homeostasis

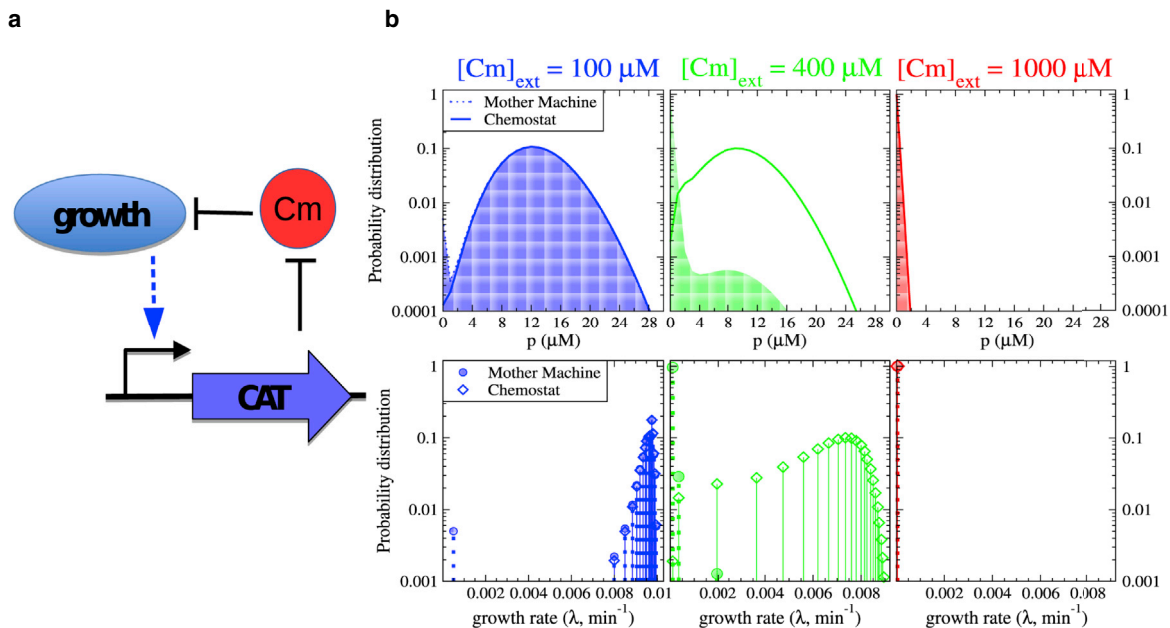


FIGURE 5 Growth bistability in an antibiotic resistance circuit. (a) Given here is the schematic representation of the growth-modulating antibiotic resistance system. (b) Shown here is the distribution of concentration of the resistance protein CAT (top) and of the growth rates of cells (bottom), as obtained from Chemostat and Mother Machine simulations for three different antibiotic concentrations. The solid curves and the diamonds with solid dropdown lines are for the Chemostat and the shaded down-curves and the shaded circles with dotted dropdown lines are for the Mother Machine. For parameter values, see the Supporting Material. The sampling is done over 1000 cells and for 10^6 time steps of 60 min each. To see this figure in color, go online.

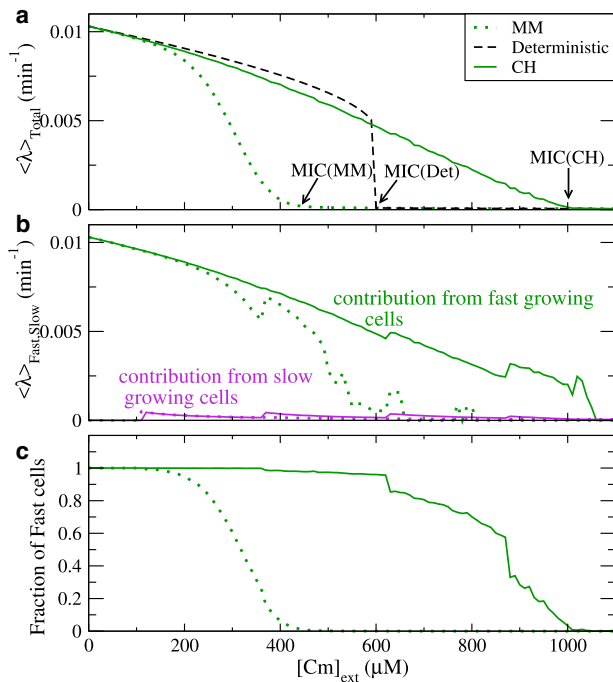


FIGURE 6 Dependence of the MIC on the population setup. (a) Shown here is the average growth rate of the population as a function of the (increasing) Cm concentration in the Chemostat (solid lines) and the Mother Machine (dotted lines). The dashed black line shows the corresponding result from the deterministic model. (b) Shown here are growth rate averages within the two subpopulations of fast growing (green) and slow growing cells (magenta). (c) Shown here are fractions of fast growing and slow growing cells in the two setups. Cells with $\lambda > 0.0005 \text{ min}^{-1}$ are taken as fast cells (we note that the jumps in b and c arise when the discrete values of the growth rate cross this cutoff upon increase of the antibiotic concentration). The averaging is done over 10,000 cells and over 10 time steps of 30 min each, after equilibrating for 1000 min in the corresponding antibiotic concentration. To see this figure in color, go online.

mechanism. In that case, the population growth rate was found to be lower than the average growth rate of the cells rather than higher. In the bistable systems we consider here, however, the growth heterogeneity is dominated by the difference in growth rate between the phenotypes, which exceeds the more subtle growth heterogeneity due to stochastic cell division control and size homeostasis in the monostable systems discussed in (39,51). As a result, the impact of the mechanism of division can be expected to be weaker than in those systems.

A bistable antibiotic-resistant system

Next, we apply our approach to growth bistability in an antibiotic resistance circuit, which has been demonstrated recently (23): for translation-targeting antibiotics, a positive feedback results from the growth modulation by a resistance gene and the growth-rate-dependent expression of that resistance gene. Specifically, we consider the constitutive expression of chloramphenicol acetyltransferase (CAT),

which modifies and deactivates the translation-targeting antibiotic chloramphenicol (Cm). Under growth modulation by translation-inhibiting antibiotics, constitutively expressed genes display a linearly increasing dependence of the concentration of their protein product on the growth rate (20). Increased expression of CAT results in a reduced intracellular concentration of Cm and thereby to an increased growth rate, establishing the positive feedback (Fig. 5 a) (see the Supporting Material for details of the model).

In Fig. 5 b, we plot distributions of the CAT concentration and of the growth rate for three different extracellular antibiotic concentrations, as obtained from simulations with the Mother Machine and Chemostat setups. For the highest of the three Cm concentrations, all cells are slow growing; for the lowest concentration, (almost) all cells are fast growing. For the intermediate concentration, the circuit is bistable, with fast growing and slow growing subpopulations. In the two monomodal situations (high and low Cm concentrations), the two population setups result in almost the same distributions, in agreement with the general picture obtained for the toggle switch example discussed above. In the bistable regime (intermediate Cm concentration), however, we see again that the results are different for the two setups: the Mother Machine has more of the slower growing cells, whereas the Chemostat has more of the faster growing cells.

The impact of the growth setup on the population structure has an important consequence for the measurement of MIC. The MIC is often determined as the concentration, where the growth rate drops abruptly to a very low value. Because, in our model, the drop is gradual rather than abrupt, we determine an MIC as the antibiotic concentration, for which the growth rate drops below 2% of the growth rate in absence of the antibiotic. As can be seen in Fig. 6 a, the MICs obtained in the two scenarios differ substantially (1000 μM for the Chemostat simulations and 450 μM for the Mother Machine). This difference reflects again that the cells in the Mother Machine population preferentially stay in the more long-lived slow growing state, whereas in the Chemostat, fast growing cells will dominate the population, whenever some of them appear (Fig. 6 c).

Conversely, the measured MIC has been used to determine parameters of the circuit (23). In doing so, one will get different results based on which growth scenario is used in the simulation one fits the experimental data with, and care has to be taken to use the growth setup matching the experimental conditions.

Experimentally, MICs are usually measured in growing populations, either in batch cultures or petri dishes rather than in a system with a fixed number of cells. We emphasize that our Chemostat simulation is designed to reflect the properties of such a growing population, despite the fact that the number of cells is constant. To check this explicitly, we also simulated a population with a growing number of

cells and determined growth rates from the growth curves. The results, including the resulting MIC, are in excellent agreement with the results from the Chemostat simulation (Fig. S8). We note that in the experiments of (23), the drop in growth rate at the MIC is sharper than in our simulations. This discrepancy is likely due to the stochastic description, possibly the relatively wide distribution of growth rates it generates (Fig. 5 b, bottom panel), as a sharp drop is also seen in the deterministic version of the same model (Fig. 6 a). However, because the dependence of the MIC on the population setup is a consequence of the different population statistics, this would also be seen in modifications of the stochastic description. We reiterate that the presence of growing cells above the MIC of the deterministic model is a result of fast growing cells replacing slow growing ones, rather than transient resistance due to stochastic gene expression (27).

Concluding remarks

In summary, we developed a computational formalism to simulate a set of reactions in a population of growing cells, implementing two types of experimental setups, the Mother Machine and the Chemostat. We also developed a modified version of Gillespie's stochastic simulation algorithm, which is extremely efficient in simulating a set of reactions that are clustered, in our case, into the different cells. With the help of two test genetic circuits, a mutual repressor with growth reduction in one state and a bistable antibiotic-resistant system, we then showed how various measurable quantities can have the distinct signature of the experimental setup being studied. This was seen to be a result of the different subpopulation structures in the different setups whenever there is heterogeneity in growth, such as the growth bistability in the two cases we studied. Specifically, we showed for the resistance circuit that the MIC of the antibiotic may depend on the experimental setup.

We expect that our method, which may be extended to other population setups, will provide a basis for future studies of any genetic circuit where growth heterogeneity has the potential to modify the subpopulation structures. With the broad current interest in microbial communities, from single-species biofilms to the diversity of the microbiome, we expect that there will be many other applications for our approach.

SUPPORTING MATERIAL

Supporting Materials and Methods and eight figures are available at [http://www.biophysj.org/biophysj/supplemental/S0006-3495\(17\)35007-5](http://www.biophysj.org/biophysj/supplemental/S0006-3495(17)35007-5).

AUTHOR CONTRIBUTIONS

A.R. and S.K. designed the research. A.R. performed the research. A.R. and S.K. wrote the manuscript.

REFERENCES

- Gardner, T. S., C. R. Cantor, and J. J. Collins. 2000. Construction of a genetic toggle switch in *Escherichia coli*. *Nature*. 403:339–342.
- Elowitz, M. B., and S. Leibler. 2000. A synthetic oscillatory network of transcriptional regulators. *Nature*. 403:335–338.
- Hasty, J., D. McMillen, and J. J. Collins. 2002. Engineered gene circuits. *Nature*. 420:224–230.
- Guido, N. J., X. Wang, ..., J. J. Collins. 2006. A bottom-up approach to gene regulation. *Nature*. 439:856–860.
- Kuhlman, T., Z. Zhang, ..., T. Hwa. 2007. Combinatorial transcriptional control of the lactose operon of *Escherichia coli*. *Proc. Natl. Acad. Sci. USA*. 104:6043–6048.
- Lin, Y., C. H. Sohn, ..., M. B. Elowitz. 2015. Combinatorial gene regulation by modulation of relative pulse timing. *Nature*. 527:54–58.
- Ozbudak, E. M., M. Thattai, ..., A. Van Oudenaarden. 2004. Multistability in the lactose utilization network of *Escherichia coli*. *Nature*. 427:737–740.
- Balaban, N. Q., J. Merrin, ..., S. Leibler. 2004. Bacterial persistence as a phenotypic switch. *Science*. 305:1622–1625.
- Chai, Y., F. Chu, ..., R. Losick. 2008. Bistability and biofilm formation in *Bacillus subtilis*. *Mol. Microbiol.* 67:254–263.
- Veening, J. W., W. K. Smits, and O. P. Kuipers. 2008. Bistability, epigenetics, and bet-hedging in bacteria. *Annu. Rev. Microbiol.* 62:193–210.
- McAdams, H. H., and A. Arkin. 1997. Stochastic mechanisms in gene expression. *Proc. Natl. Acad. Sci. USA*. 94:814–819.
- Elowitz, M. B., A. J. Levine, ..., P. S. Swain. 2002. Stochastic gene expression in a single cell. *Science*. 297:1183–1186.
- Raser, J. M., and E. K. O'Shea. 2005. Noise in gene expression: origins, consequences, and control. *Science*. 309:2010–2013.
- Kaern, M., T. C. Elston, ..., J. J. Collins. 2005. Stochasticity in gene expression: from theories to phenotypes. *Nat. Rev. Genet.* 6:451–464.
- Raj, A., and A. van Oudenaarden. 2008. Nature, nurture, or chance: stochastic gene expression and its consequences. *Cell*. 135:216–226.
- Klumpp, S., and T. Hwa. 2014. Bacterial growth: global effects on gene expression, growth feedback and proteome partition. *Curr. Opin. Biotechnol.* 28:96–102.
- Schaechter, M., O. Maaloe, and N. O. Kjeldgaard. 1958. Dependency on medium and temperature of cell size and chemical composition during balanced growth of *Salmonella typhimurium*. *J. Gen. Microbiol.* 19:592–606.
- Bremer, H., and P. P. Dennis. 1996. Modulation of chemical composition and other parameters of the cell by growth rate. In *Escherichia coli and Salmonella*. F. C. Neidhardt, ed. ASM Press, Washington, D.C., pp. 1553–1569.
- Klumpp, S., Z. Zhang, and T. Hwa. 2009. Growth rate-dependent global effects on gene expression in bacteria. *Cell*. 139:1366–1375.
- Scott, M., C. W. Gunderson, ..., T. Hwa. 2010. Interdependence of cell growth and gene expression: origins and consequences. *Science*. 330:1099–1102.
- Weiße, A. Y., D. A. Oyarzún, ..., P. S. Swain. 2015. Mechanistic links between cellular trade-offs, gene expression, and growth. *Proc. Natl. Acad. Sci. USA*. 112:E1038–E1047.
- Tan, C., P. Marguet, and L. You. 2009. Emergent bistability by a growth-modulating positive feedback circuit. *Nat. Chem. Biol.* 5:842–848.
- Deris, J. B., M. Kim, ..., T. Hwa. 2013. The innate growth bistability and fitness landscapes of antibiotic-resistant bacteria. *Science*. 342:1237435.
- Berthoumieux, S., H. de Jong, ..., J. Geiselmann. 2013. Shared control of gene expression in bacteria by transcription factors and global physiology of the cell. *Mol. Syst. Biol.* 9:634.

25. Gerosa, L., K. Kochanowski, ..., U. Sauer. 2013. Dissecting specific and global transcriptional regulation of bacterial gene expression. *Mol. Syst. Biol.* 9:658.
26. Rotem, E., A. Loinger, ..., N. Q. Balaban. 2010. Regulation of phenotypic variability by a threshold-based mechanism underlies bacterial persistence. *Proc. Natl. Acad. Sci. USA.* 107:12541–12546.
27. El Meouche, I., Y. Siu, and M. J. Dunlop. 2016. Stochastic expression of a multiple antibiotic resistance activator confers transient resistance in single cells. *Sci. Rep.* 6:19538.
28. Burrill, D. R., and P. A. Silver. 2011. Synthetic circuit identifies subpopulations with sustained memory of DNA damage. *Genes Dev.* 25:434–439.
29. Nevozhay, D., R. M. Adams, ..., G. Balázsi. 2012. Mapping the environmental fitness landscape of a synthetic gene circuit. *PLoS Comput. Biol.* 8:e1002480.
30. Monod, J. 1949. The growth of bacterial cultures. *Annu. Rev. Microbiol.* 3:371–394.
31. Jordan, R. C., S. E. Jacobs, and A. L. Sims. 1944. The growth of bacteria with a constant food supply: I. Preliminary observations on *Bacterium coli*. *J. Bacteriol.* 48:579–598.
32. Herbert, D., R. Elsworth, and R. C. Telling. 1956. The continuous culture of bacteria; a theoretical and experimental study. *J. Gen. Microbiol.* 14:601–622.
33. Wheeler, A. R., W. R. Thronset, ..., A. Daridon. 2003. Microfluidic device for single-cell analysis. *Anal. Chem.* 75:3581–3586.
34. Long, Z., E. Nugent, ..., K. D. Dorfman. 2013. Microfluidic chemostat for measuring single cell dynamics in bacteria. *Lab Chip.* 13:947–954.
35. Wang, P., L. Robert, ..., S. Jun. 2010. Robust growth of *Escherichia coli*. *Curr. Biol.* 20:1099–1103.
36. Taheri-Araghi, S., S. Bradde, ..., S. Jun. 2015. Cell-size control and homeostasis in bacteria. *Curr. Biol.* 25:385–391.
37. Hasty, J., D. McMillen, ..., J. J. Collins. 2001. Computational studies of gene regulatory networks: in numero molecular biology. *Nat. Rev. Genet.* 2:268–279.
38. Gomez, D., R. Marathe, ..., S. Klumpp. 2014. Modeling stochastic gene expression in growing cells. *J. Theor. Biol.* 348:1–11.
39. Hashimoto, M., T. Nozoe, ..., Y. Wakamoto. 2016. Noise-driven growth rate gain in clonal cellular populations. *Proc. Natl. Acad. Sci. USA.* 113:3251–3256.
40. Gillespie, D. T. 1976. A general method for numerically simulating the stochastic time evolution of coupled chemical reactions. *J. Comput. Phys.* 22:403–434.
41. Gillespie, D. T. 1977. Exact stochastic simulation of coupled chemical reactions. *J. Phys. Chem.* 81:2340–2361.
42. Moran, P. A. P. 1958. Random processes in genetics. *Proc. Camb. Philos. Soc.* 54:60–71.
43. Gillespie, D. T. 2007. Stochastic simulation of chemical kinetics. *Annu. Rev. Phys. Chem.* 58:35–55.
44. Gibson, M. A., and J. Bruck. 2000. Efficient exact stochastic simulation of chemical systems with many species and many channels. *J. Phys. Chem. A.* 104:1876–1889.
45. Sedgewick, R. 1998. Algorithms in C. Addison-Wesley, Reading, MA.
46. Lok, L., and R. Brent. 2005. Automatic generation of cellular reaction networks with Molecuizer 1.0. *Nat. Biotechnol.* 23:131–136.
47. Cao, Y., H. Li, and L. Petzold. 2004. Efficient formulation of the stochastic simulation algorithm for chemically reacting systems. *J. Chem. Phys.* 121:4059–4067.
48. McCollum, J. M., G. D. Peterson, ..., N. F. Samatova. 2006. The sorting direct method for stochastic simulation of biochemical systems with varying reaction execution behavior. *Comput. Biol. Chem.* 30:39–49.
49. Patra, P., and S. Klumpp. 2013. Population dynamics of bacterial persistence. *PLoS One.* 8:e62814.
50. Hintsche, M., and S. Klumpp. 2013. Dilution and the theoretical description of growth-rate dependent gene expression. *J. Biol. Eng.* 7:22.
51. Lin, J., and A. Amir. 2017. The effect of stochasticity at the single-cell level and cell size control on the population growth. *Cell Syst.* 5:358–367.e4.

Biophysical Journal, Volume 114

Supplemental Information

**Simulating Genetic Circuits in Bacterial Populations with Growth
Heterogeneity**

Anjan Roy and Stefan Klumpp

Simulation algorithm

All simulations are run with different versions of Gillespie's stochastic simulation algorithm [1, 2]. In these simulations, the dynamics of the various reaction channels are characterized by their propensities a_j . These propensities determine the probabilities of the time τ when the next reaction will take place, given by the probability density $p(\tau) = a \exp(-a\tau)$, where $a = \sum_j a_j$ is the sum of propensities, and which of the reactions is chosen, determined by the probabilities $p(j) = a_j/a$. In the Direct Method (which we use here for comparison) we draw two random numbers r_1 and r_2 from a uniform distribution on the unit interval and calculate the time of the next reaction as $\tau = t + \frac{1}{a} \ln(\frac{1}{r_1})$ and the index of the next reaction as $j =$ the smallest integer satisfying $\sum_{j'=1}^j a_{j'}/a > r_2$. With this we proceed the time of the simulation to $t = \tau$, carry out the reaction j , record the desired quantities and calculate new set of propensities for the next reaction.

In the Next Family Method we group the reactions into families; each family consists of the reactions of one cell. These families are then considered as pseudo-reactions with propensities $a^f = \sum_{j=1}^{l^f} a_j^f$, where l^f is the number of reactions in the family/cell f . Next, we generate the expected times of the next reaction for each family as $\tau^f = t + \frac{1}{a^f} \ln(\frac{1}{r_1})$ and heapify these so that they are in a tree-ordered data structure, in which the node representing the family (say m) is the one with the smallest time τ^m [3]. This gives us the time of the next reaction in the population as $t = \tau^m$ and the cell in which the reaction is happening as m . To obtain the actual reaction that is firing we apply the Direct Method to the l^m reactions in this family. With this we then proceed the time of the simulation to $t = \tau^m$, implement that reaction, sample the desired quantities, calculate the new set of propensities (a_{new}^m) and repair the heap starting from this nodal position based on its new expected time for the next reaction, $\tau_{new}^m = t + \frac{1}{a_{new}^m} \ln(\frac{1}{r_1})$. If no other cell is affected by this reaction, we do not have to do any other heap repair step and can read off the time and index of the next reaction in the population from the updated heap in similar way. For the Chemostat, if the next reaction happens to be the production of a daughter cell, we produce a copy of the dividing cell and replace a randomly chosen cell (say r_3) with it. In this case the heap has to be repaired starting at the position of the cell r_3 . To obtain this position we use indexed heap data structure so that if the heap consists of ordered pairs (f, τ^f) , the

f -th element of the index structure will point to the position of the (f, τ^f) pair in the heap.

Mutual repressor system with growth inhibition

In a simple Mutual Repressor the deterministic equations for the evolution of the concentrations of the two proteins p_i are given by

$$\begin{aligned}\frac{dp_1}{dt} &= \alpha_1 \frac{1}{1 + (p_2/K_2)^{n_2}} - (\beta_{01} + \lambda)p_1 \\ \frac{dp_2}{dt} &= \alpha_2 \frac{1}{1 + (p_1/K_1)^{n_1}} - (\beta_{02} + \lambda)p_2\end{aligned}\quad (1)$$

where α_i are the synthesis rates of the proteins, β_{0i} are the degradation rates due to proteolysis and λ is the growth rate, related to cell division time T_d as $\lambda = \ln 2/T_d$. Note that here we have described the two step protein synthesis process, involving transcription and translation, as an effective one step process. Moreover, it is an implicit cell division model where we include the dilution rate due to cell growth and division into the degradation term, i.e., we study the effective average behavior in the cell at times longer than the cell division time. K_i are the threshold concentrations for repression and n_i , the Hill coefficients, represent the cooperativity of binding needed for repression, both being determined by the architecture of the corresponding promoter regions.

The above system is known to exhibit bistability for $n_i \geq 2$. To incorporate a difference in growth rates between the two states, we assume the protein P_1 to be inhibitory to the growth of the cell. We model this toxicity to growth as

$$\lambda = \lambda_{min} + \frac{\Delta\lambda}{(1 + p_1/K_\lambda)}, \quad (2)$$

where $\Delta\lambda = (\lambda_{max} - \lambda_{min})$ and K_λ is the characteristic concentration for the protein to be toxic. To study phenotype switching, we treat the above set of equations as a stochastic chemical reaction system and simulate it with the Stochastic Simulation Algorithm described above. The propensities for this system are given as $a_1 = \alpha_1 \frac{1}{1 + (p_2/K_2)^{n_2}}$, $a_2 = \alpha_2 \frac{1}{1 + (p_1/K_1)^{n_1}}$, $a_3 = (\beta_{01} + \lambda)p_1$ and $a_4 = (\beta_{02} + \lambda)p_2$. λ is instantaneously determined by Eq. 2. The parameters used are $\alpha_1 = \alpha_2 = 3 \mu M \text{ min}^{-1}$, $\beta_{01} = \beta_{02} = 0.005 \text{ min}^{-1}$, $K_i = K_\lambda = 20 \mu M$, $\lambda_{max} = 0.04 \text{ min}^{-1}$. λ_{min} is varied to modulate the toxicity.

In the more realistic case, the synthesis rate is taken to depend on the growth rate of the

cell using the expression from ref. [4]

$$\begin{aligned}\frac{dp_1}{dt} &= \frac{\alpha_1[1 - \exp(-\lambda/\lambda')]}{1 + (p_2/K_2)^{n_2}} - \beta_1 p_1 \\ \frac{dp_2}{dt} &= \frac{\alpha_2[1 - \exp(-\lambda/\lambda')]}{1 + (p_1/K_1)^{n_1}} - \beta_2 p_2.\end{aligned}\quad (3)$$

The toxicity is described by

$$\lambda = \frac{\lambda_{max}}{(1 + p_1/K_\lambda)}.\quad (4)$$

and varied by modulating the threshold concentration K_λ . The parameter values are given in the caption of Fig. S6.

Bistable antibiotic resistance circuit

The bistable resistance circuit described in Ref. [5] is based on a positive feedback in which expression of a resistance gene reduces the intracellular antibiotic concentration. The latter reduction speeds up growth, which has a positive effect on expression of the resistance gene, because growth in translation-limited conditions increases the expression of constitutively expressed genes [6] such as the resistance gene. The three components of that positive feedback are described as follows: The growth rate of the cell in the presence of antibiotic is given by

$$\lambda = \frac{\lambda_0}{(1 + [\text{Cm}]_{\text{int}}/I_{50})},$$

where λ_0 is the growth rate in the absence of intracellular antibiotic and I_{50} is the concentration of intracellular antibiotic that reduces the growth rate by half. $[\text{Cm}]_{\text{int}}$ is the concentration of the antibiotic inside the cell, which is obtained from the extracellular concentration by balancing its diffusion in and out of the cell with its degradation or deactivation by the resistance protein CAT. This balance is given by

$$\begin{aligned}\kappa([\text{Cm}]_{\text{ext}} - [\text{Cm}]_{\text{int}}) &= \frac{k_c p}{1 + K_m/[\text{Cm}]_{\text{int}}} \\ \text{or, } [\text{Cm}]_{\text{int}} &= \frac{1}{2} \left[[\text{Cm}]_{\text{ext}} - \left(K_m + \frac{k_c}{\kappa} p\right) + \sqrt{\left(K_m + \frac{k_c}{\kappa} p - [\text{Cm}]_{\text{ext}}\right)^2 + 4K_m[\text{Cm}]_{\text{ext}}} \right],\end{aligned}$$

where κ is the permeability of the cell membrane to Cm, K_m is the affinity of CAT to Cm, k_c the maximal rate of turnover of Cm by CAT, and p is the concentration of CAT.

The expression levels of unregulated proteins in the cell depend linearly on the growth rate of the cell under sub-inhibitory concentrations of translation-inhibiting antibiotics, so that

$$p = \frac{p_0}{\lambda_0} \lambda,$$

where quantities with suffix 0 indicate values in the absence of the antibiotic. This dependence is included in the model by choosing the synthesis rates as a quadratic function of the growth rate. Similar to the model of the toggle switch, we formulate a deterministic rate equation as

$$\frac{dp}{dt} = \alpha \lambda^2 - (\beta_0 + \lambda)p,$$

with $\alpha = p_0/\lambda_0$, so that now the propensities for the stochastic simulation are $a_1 = \alpha \lambda^2$ and $a_2 = (\beta_0 + \lambda)p$. We simulate the above set of equations in the same way as for the previous model, with λ and $[Cm]_{\text{int}}$ taken as instantaneous quantities. The model parameters are obtained from Table S2 of Ref. [5] as $\lambda_0 = 0.01 \text{ min}^{-1}$, $I_{50} = 5.5 \text{ } \mu\text{M}$, $K_m = 12 \text{ } \mu\text{M}$, $k_c = 36000 \text{ min}^{-1}$, $p_0 = 14.2 \text{ } \mu\text{M}$ for the strain Cat1; β_0 was set to a small non-zero value, $\beta_0 = 0.0002 \text{ min}^{-1}$ and κ was taken to be 126 min^{-1} to match the MIC in the Chemostat simulation to the experimentally observed value.

-
- [1] Gillespie, D. T. (1976). A general method for numerically simulating the stochastic time evolution of coupled chemical reactions. *J. Comput. Phys.* 22, 403-434.
 - [2] Gillespie, D. T. (1977). Exact stochastic simulation of coupled chemical reactions. *J. Phys. Chem.* 81, 2340-2361.
 - [3] Sedgewick, R. (1998). *Algorithms in C*. Addison-Wesley, Reading.
 - [4] Hintsche, M., Klumpp, S. (2013). Dilution and the theoretical description of growth-rate dependent gene expression. *J. Biol. Eng.* 7, 22.
 - [5] Deris, J. B., Kim, M., Zhang, Z., Okano, H., Hermsen, R., Groisman, A., Hwa, T. (2013). The innate growth bi-stability and fitness landscapes of antibiotic-resistant bacteria. *Science* 342, 1237435.
 - [6] Scott, M., Gunderson, C. W., Mateescu, E. M., Zhang, Z., Hwa, T. (2010) Inter-dependence of cell growth and gene expression: Origins and consequences. *Science* 330, 1099-1102.

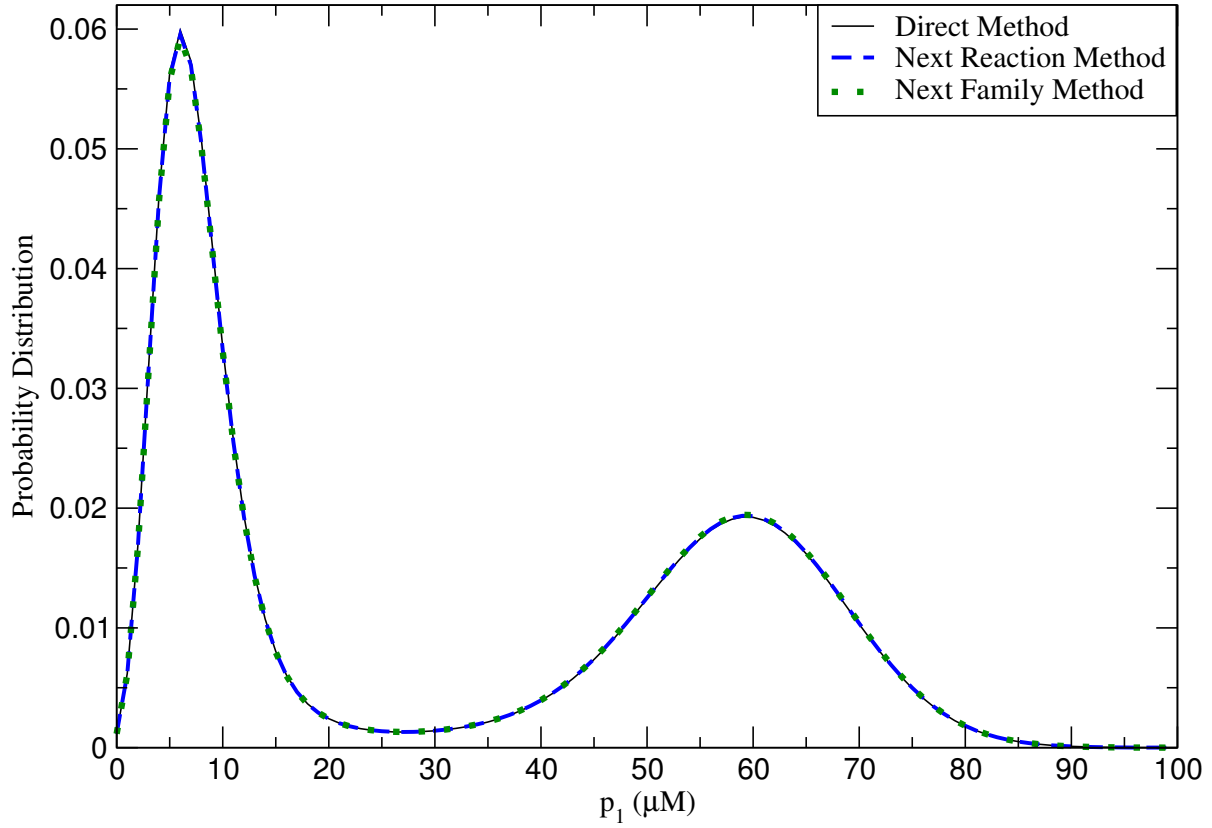


FIG. S1. Distribution of protein concentration obtained from the three methods are statistically identical. Here, the sampling is done over 10^6 steps of 5 min each after 1000 min of equilibration (i.e. for 5,001,000 min) and over 1000 cells.

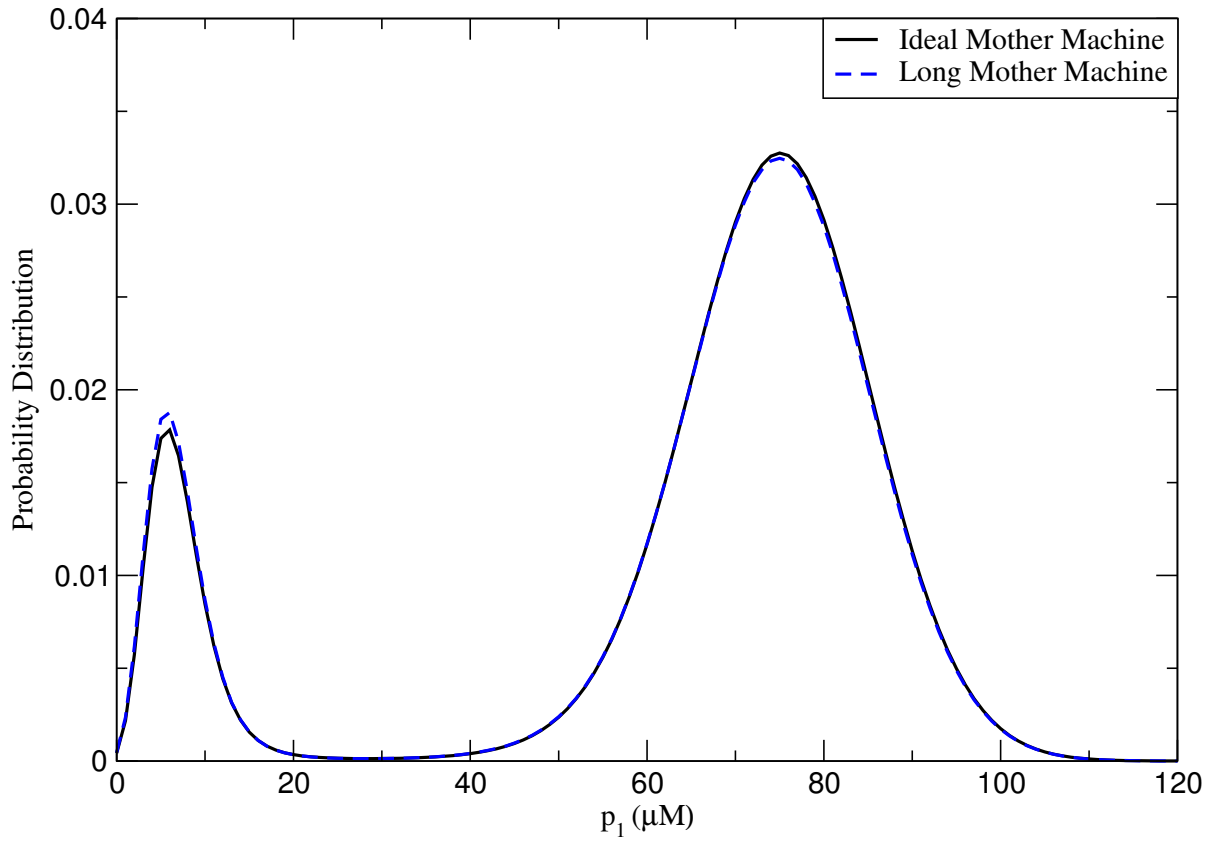


FIG. S2. Distribution of protein concentration obtained in the ideal Mother Machine is qualitatively similar to that in a 20 cell long channel Mother Machine. Here the results are for the case where P_1 is toxic so that high p_1 state is more probable.

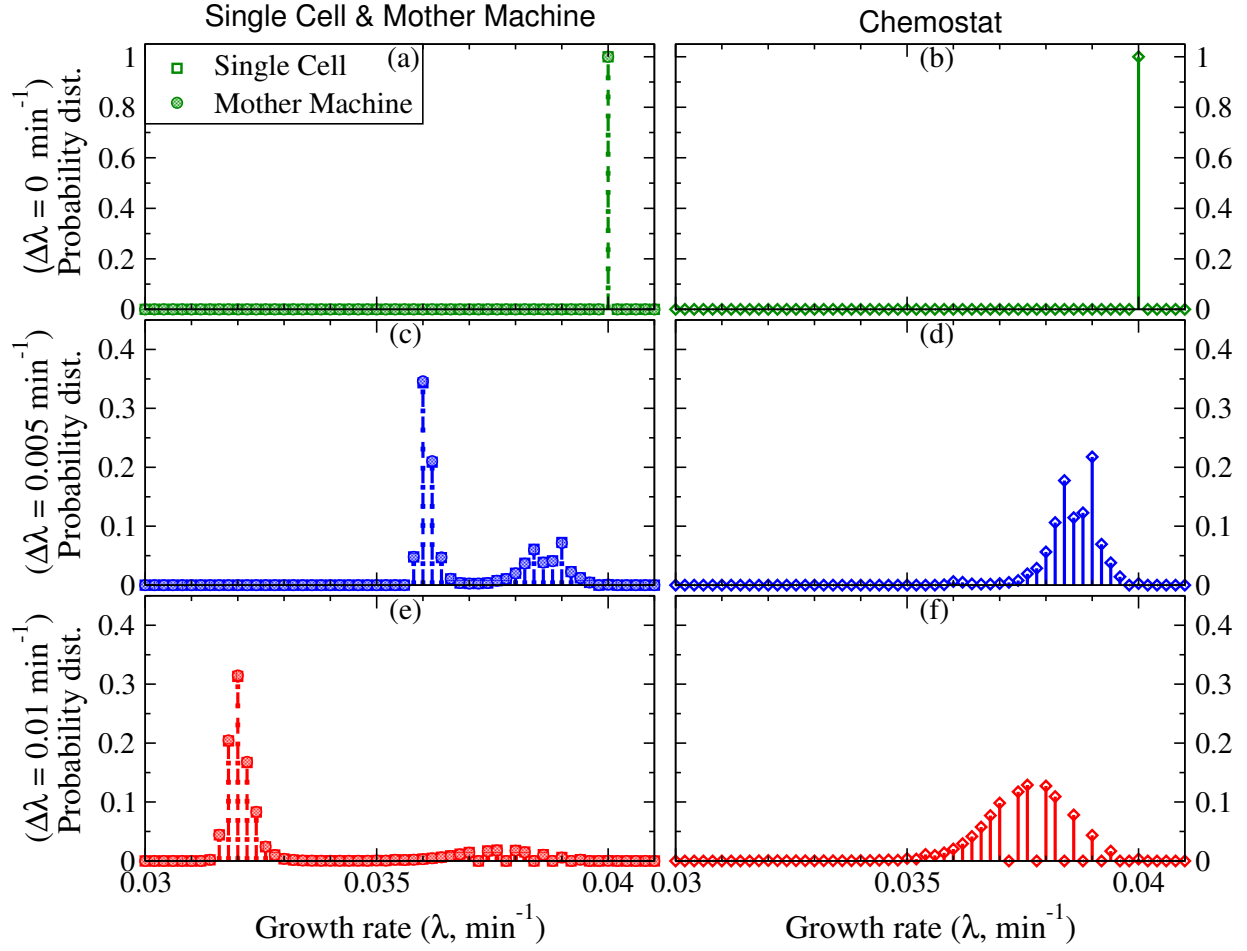


FIG. S3. Distribution of growth rates for the toxic toggle switch in a single cell (squares with dashed dropdown lines) and in the two population setups (shaded circles with dotted dropdown lines for the Mother Machine and diamonds with solid dropdown lines for the Chemostat). The parameters are the same as in Fig. 4. A bin of 0.002 min^{-1} has been used.

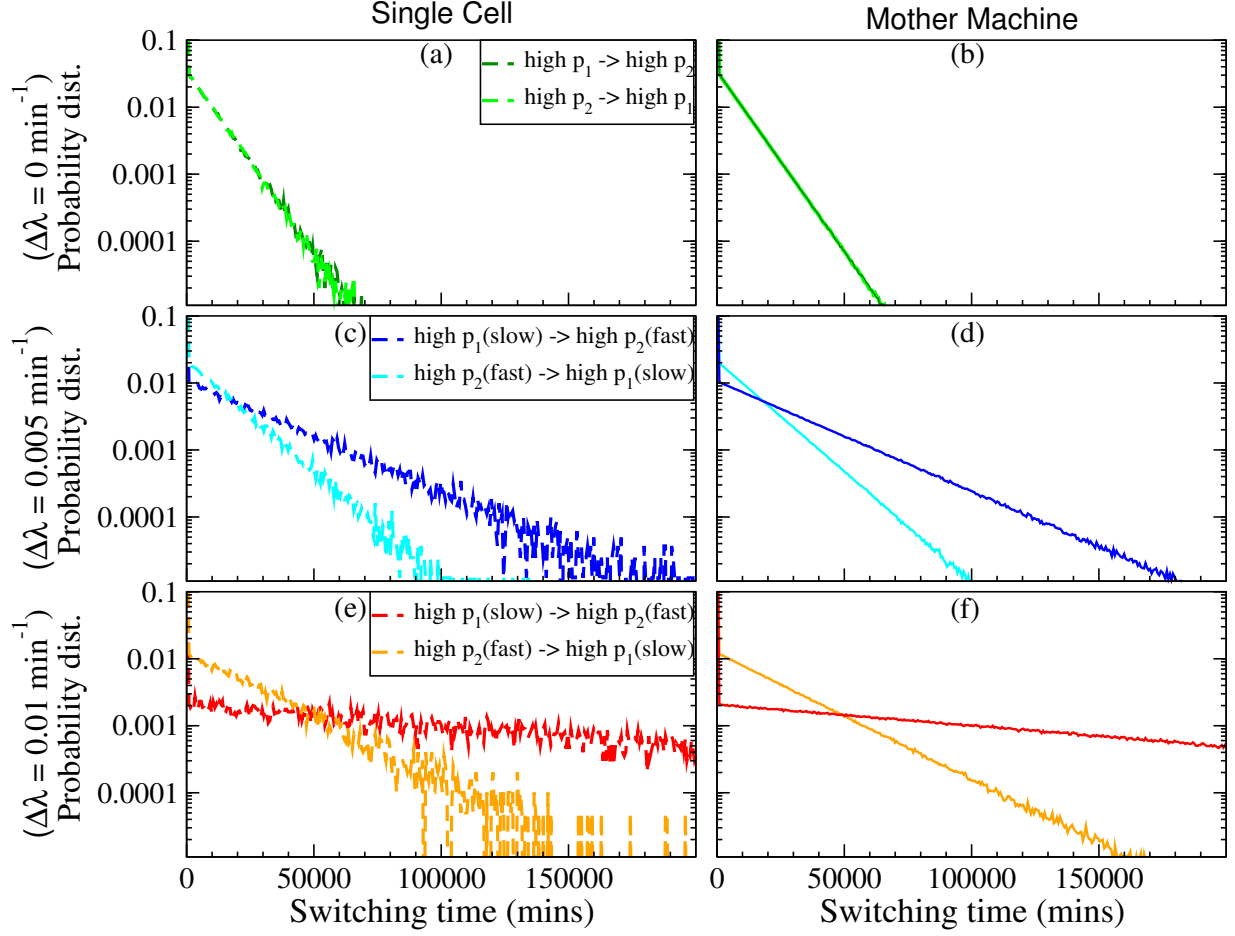


FIG. S4. Distribution of phenotype switching times for the toxic toggle switch: switching times from slow growing to fast growing (dark green, blue, red) and from fast growing to slow growing (light green, cyan, orange) states, for a single cell (dashed curves) and for the Mother Machine population (solid curves). The sampling is done over 10^8 time steps of 15 min each for the single cell, and over 1000 cells and 10^7 time steps of 15 min each for the Mother Machine population. A bin of 600 min has been used.

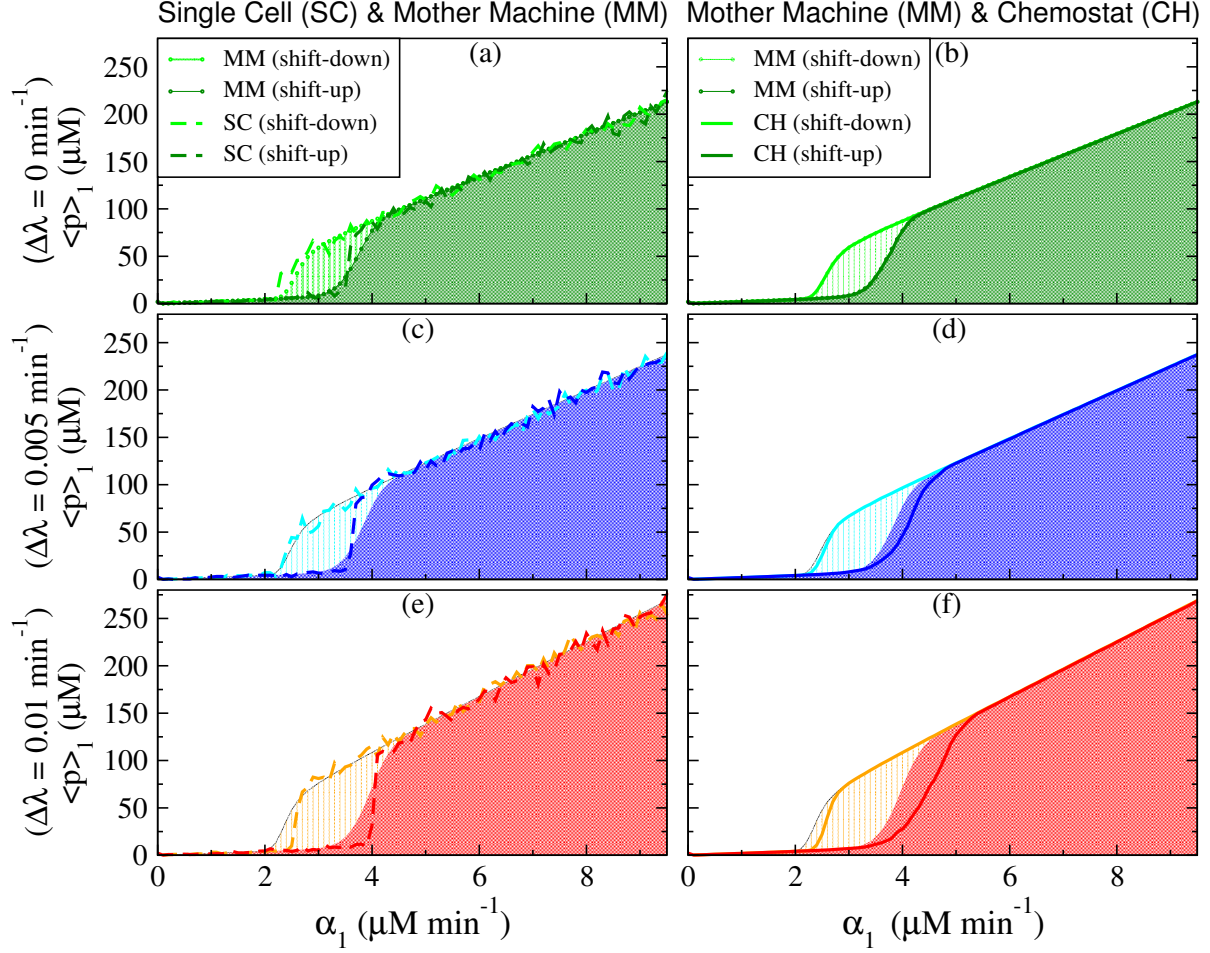


FIG. S5. Hysteresis curves for the toxic toggle switch: Hysteresis plots for the concentration of protein P_1 as its synthesis rate is varied (dark green, blue, red for shift up of the synthesis rate and light green, cyan, orange for shift down). The dashed curves are for the single cell, the shaded down curves are for the Mother Machine and the solid curves are for the Chemostat. The averaging is done for 100 steps of 2 min each for the Single cell. For the two populations a further averaging over 10000 cells has been done. We note that the noise in the single cell plots is because of averaging over a small time. Averaging over times longer than switching times will collapse the hysteresis curves. This further highlights the advantage of having the possibility to average over many cells in the Mother Machine, even for studying single cell statistics.

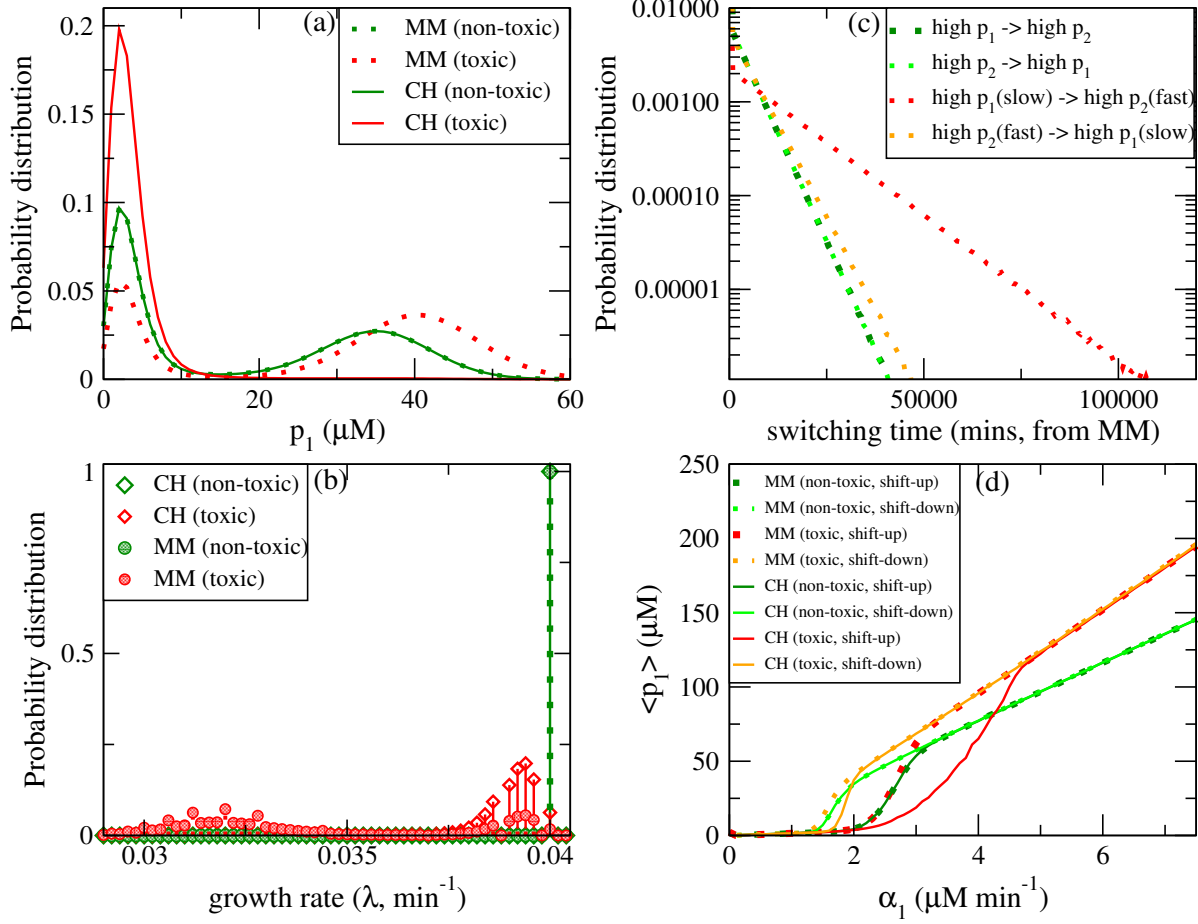


FIG. S6. Results for a more realistic model of toxic toggle switch: The toggle switch model with growth inhibition by one of the two proteins (P_1) is extended to include a growth-rate dependence of the synthesis rates; growth inhibition is modulated by varying the threshold concentration in a repression function. Distributions of (a) the concentration of the protein P_1 , (b) of the growth rate (green curves are without growth inhibition (infinite K_λ , non-toxic), red curves are with growth inhibition ($K_\lambda = 160 \mu M$, toxic)) and (c) of the switching times from slow growing to fast (dark green, red) and from fast growing to slow (light green, orange). (d) Hysteresis curves upon variation of the synthesis rate of protein P_1 (dark green and red curves for shift-up and light green and orange for shift-down). The parameters are $\alpha_1 = \alpha_2 = 2 \mu M \text{ min}^{-1}$, $\beta_{01} = \beta_{02} = 0.005 \text{ min}^{-1}$, $K_1 = K_2 = 10 \mu M$, $\lambda_{max} = 0.04 \text{ min}^{-1}$, $\lambda' = 0.02 \text{ min}^{-1}$. Dotted curves are for the Mother Machine population, while the solid curves are for the Chemostat population. Parameters for averaging and binning are the same as in the corresponding figures of the simple toxic toggle switch.

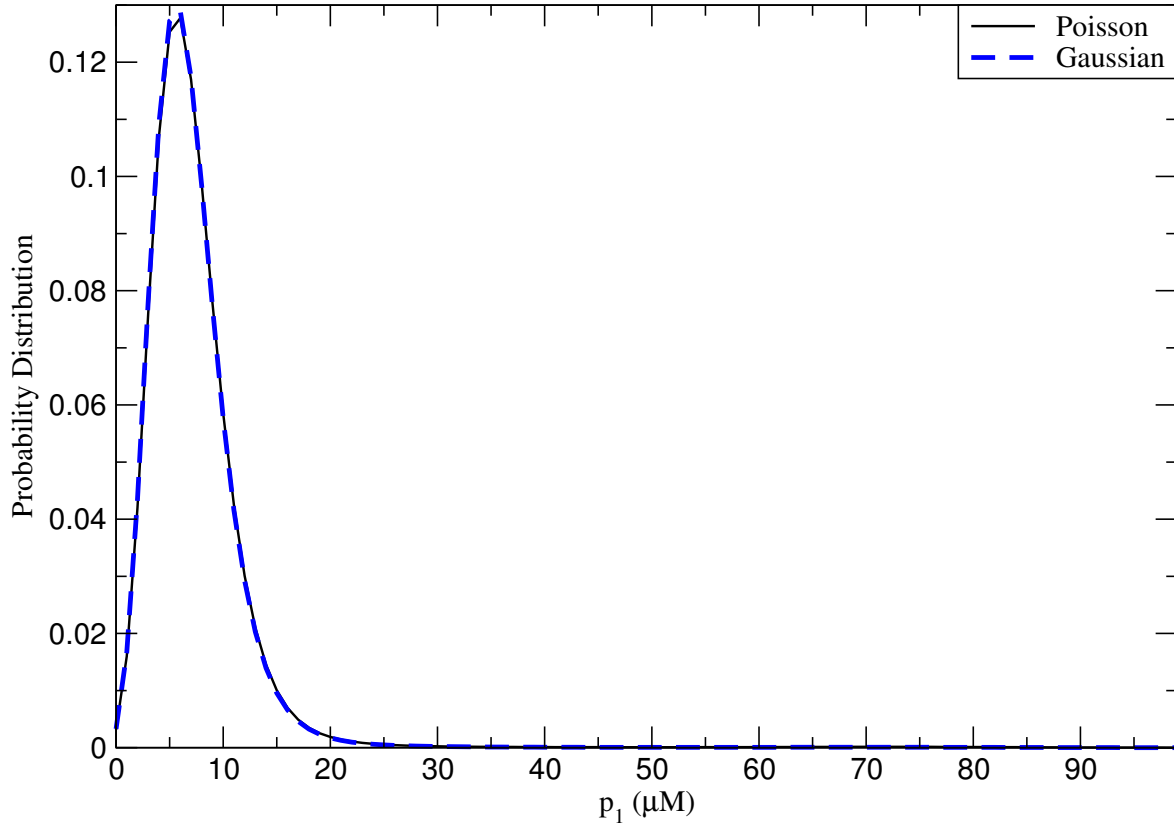


FIG. S7. Distribution of protein concentration obtained by selecting division times from an uncorrelated Gaussian distribution is qualitatively similar to that obtained by selecting from an uncorrelated exponential distribution as in Poisson processes. The result is for the simple toxic toggle switch with $\Delta\lambda = 0.01 \text{ min}^{-1}$.

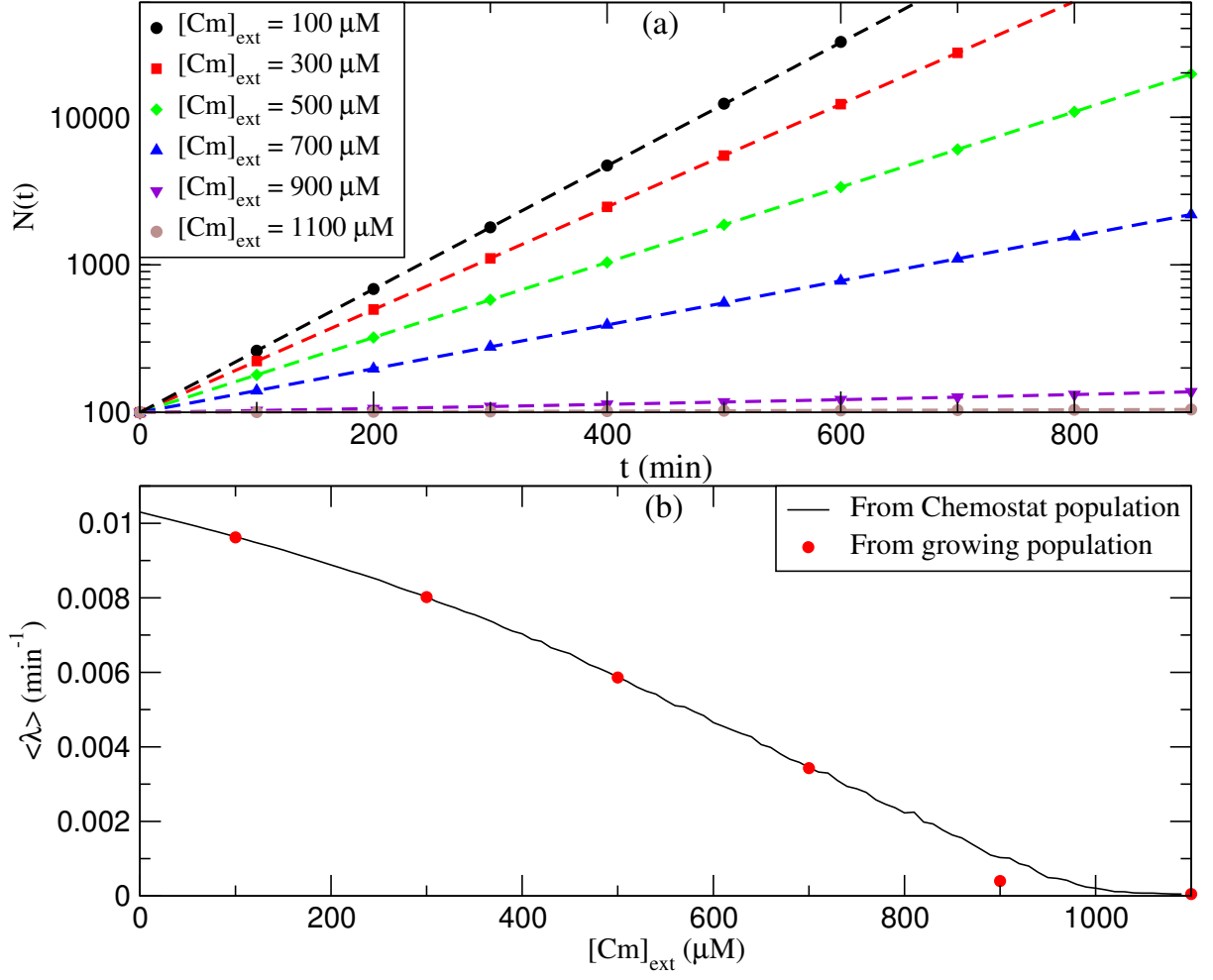


FIG. S8. Growth curve obtained from a growing population gives similar result to that obtained from the Chemostat population : (a) The system is equilibrated at different antibiotic concentrations and then grown for 900 min, starting from 100 cells. The result plotted is average over 1000 such realizations. (b) The average growth rates at each antibiotic concentrations is obtained by fitting an exponential to the curves in (a).